ADVANCED MATERIALS
www.advmat.de

Single-Junction Organic Photovoltaic Cells with Approaching 18% Efficiency

Yong Cui, Huifeng Yao, Jianqi Zhang, Kaihu Xian, Tao Zhang, Ling Hong, Yuming Wang, Ye Xu, Kangqiao Ma, Cunbin An, Chang He, Zhixiang Wei, Feng Gao, and Jianhui Hou*

Optimizing the molecular structures of organic photovoltaic (OPV) materials is one of the most effective methods to boost power conversion efficiencies (PCEs). For an excellent molecular system with a certain conjugated skeleton, fine tuning the alky chains is of considerable significance to fully explore its photovoltaic potential. In this work, the optimization of alkyl chains is performed on a chlorinated nonfullerene acceptor (NFA) named BTP-4Cl-BO (a Y6 derivative) and very impressive photovoltaic parameters in OPV cells are obtained. To get more ordered intermolecular packing, the n-undecyl is shortened at the edge of BTP-eC11 to n-nonyl and n-heptyl. As a result, the NFAs of BTP-eC9 and BTP-eC7 are synthesized. The BTP-eC7 shows relatively poor solubility and thus limits its application in device fabrication. Fortunately, the BTP-eC9 possesses good solubility and, at the same time, enhanced electron transport property than BTP-eC11. Significantly, due to the simultaneously enhanced short-circuit current density and fill factor, the BTP-eC9-based single-junction OPV cells record a maximum PCE of 17.8% and get a certified value of 17.3%. These results demonstrate that minimizing the alkyl chains to get suitable solubility and enhanced intermolecular packing has a great potential in further improving its photovoltaic performance.

Dr. Y. Cui, Dr. H. Yao, K. Xian, T. Zhang, L. Hong, Y. Wang, Y. Xu, K. Ma, Dr. C. An, Prof. C. He, Prof. J. Hou
State Key Laboratory of Polymer Physics and Chemistry
Beijing National Laboratory for Molecular Sciences
CAS Research/Education Center for Excellence in Molecular Sciences
Institute of Chemistry
Chinese Academy of Sciences
Beijing 100190, China
E-mail: yaohf@iccas.ac.cn

Dr. Y. Cui, K. Xian, L. Hong, Y. Xu, Prof. Z. Wei, Prof. J. Hou
University of Chinese Academy of Sciences
Beijing 100049, China

Dr. J. Zhang, Prof. Z. Wei
CAS Key Laboratory of Nanosystem and Hierarchical Fabrication
CAS Center for Excellence in Nanoscience
National Center for Nanoscience and Technology
Beijing 100190, China

Y. Wang, Prof. F. Gao
Department of Physics
Chemistry and Biology
Linköping University
Linköping, Sweden

The ORCID identification number(s) for the author(s) of this article can be found under https://doi.org/10.1002/adma.201908205.

DOI: 10.1002/adma.201908205

Organic photovoltaic (OPV) cells have unique features such as flexibility, lightweight, nontoxic, transparency,[1–4] and large-area OPV panels can be fabricated by low-cost solution processing methods.[5,6] These advantages promise that they have great potential applications that are complementing well with the traditional silicon-based OPV cells.[7] Over the last three decades, tremendous efforts have been devoted to the development of new materials and achieved great progress.[5,8–11] For example, in early studies, the bulk heterojunction layers employed homopolymers like poly(3-hexylthiophene) and fullerene derivatives like [6,6]-phenyl-C61 or C71-butyric acid methyl ester (PCBM) as donors and acceptors, respectively.[12–14] As they have inefficient utilization of the solar photons, the corresponding OPV cells only delivered power conversion efficiencies (PCEs) of 4–5%.[15,16] Around 2000, it was of great significance to introduce donor–acceptor concept into the molecular design of polymer donors, leading to great tunability of optical absorption and energy level alignment.[17–19] By cooperating with PCBM, the resulting OPV cells obtained over 10% PCEs and meanwhile faced huge challenges in further improvement due to the large intrinsic energy losses (E_{loss}s, usually over 0.8 eV).[20–22] Since 2015, the donor–acceptor concept was incorporated into designing nonfullerene acceptors (NFAs) like ITIC.[9,23] The E_{loss}s of NFA-based OPV cells were significantly suppressed to below 0.7 eV and thus improved the PCEs to ≈15%.[24] Recently, an NFA named Y6 and its derivatives attracted numerous attention due to their excellent photovoltaic performance.[25–29] At present, the cutting-edge OPV cells based on Y6-system have yielded PCEs of over 16%,[30–35] showing great potential in commercial applications. These advances are very encouraging and meanwhile bring a critical question that how to further improve the PCEs by designing new materials.

For organic semiconductors, the alkyl chains have crucial impacts on the intermolecular packing and charge transport.[31,36–39] For an excellent conjugated skeleton, it is crucial to fully optimize the alkyl chains to fully explore its advantage in improving the device performance of the corresponding electronics. For instance, in 2012, Pei and coworkers demonstrated that the branching position of alkyl chains could affect

the stacking conformation and thus have a great influence on the charge mobility of the resulting materials.[40] For OPV materials, the domain spacing and purity of polymer:PCBM based blend films could be modulated by subtle changes of the alkyl chains in the PffBT4T-based polymer system. As a result, the polymer with optimal alkyl chains yielded an impressive PCE of 11.7%, which is among the top values for fullerene-based OPV cells.[41] Recently, to optimize the NFA Y6, Zou et al. applied the branching strategy to tune the central alkyl chain on the pyrrole ring. They found that the third-position branched alkyl chains could get the best PCE of 16.74%.[31] It should be noted that beyond the central alkyl chains, the bithiophene units on the edge also have two alkyl chains with electron carbon atoms, which are special positions and seldom used in other NFAs. Therefore, finely optimizing these alkyl chains may have the potential to further improve the photovoltaic performance of the OPV cells.

In this work, we conduct the optimization of alkyl chains on the edge of this kind of NFA and study their applications in OPV cells. We shorten the *n*-undecyl (C11) to *n*-nonyl (C9) and then to *n*-heptyl (C7). As a result, we synthesized the NFAs of BTP-eC9 and BTP-eC7. In comparison with BTP-eC11, the BTP-eC9 with shorter alkyl chains shows suitable solubility, decreased Urbach energy, and enhanced electron mobility. Significantly, ascribed to the improved short-circuit current density (J_{SC}) and fill factor (FF), the single-junction OPV cells based on BTP-eC9 record a maximum PCE of 17.8% (17.4 ± 0.2%) and certified value of 17.3%, which are among the top values in OPV cells. Further decreasing the alkyl chain results in a low solubility and thus bad processability and photovoltaic application for BTP-eC7. These results suggest that superior photovoltaic performance can be obtained by subtlety optimizing the alkyl chains. We anticipate that higher PCEs will be achieved by further optimization of donor materials or device engineerings like multiple-compound blending and morphology control.

In the past year, the NFAs based on Y6 system have attracted numerous attention due to its excellent photovoltaic performance. The molecular configuration of Y6 is shown in **Figure 1**, which can be divided into two main parts: the rigid backbone and flexible alkyl chains. The conjugated π-backbone determines the most pronounced electronic properties like charge density distribution and frontier orbits. For Y6 molecule, it is not easy to get various modifications on the conjugated moiety as there are very limited active positions from the point view of chemistry. From the side-view of Y6, a clear twist of ≈15° is observed for the backbone, which may be caused by the steric hindrance of bulky 2-ethylhexy (EH) chain. To get optimal photovoltaic property of this kind of NFA (Figure S1, Supporting Information), finely tuning the flexible alkyl chains is highly required.

As illustrated in Figure 1, in our work, we conducted a three-step modification on Y6. First, we replaced the fluorine atoms on the terminal electron-withdrawing units with chlorine atoms to prepare the BTP-4Cl.[30] The results suggested that chlorination is more effective than fluorination in extending the optical absorption. In the BTP-4Cl-containing OPV cells, higher open-circuit voltages (V_{OC}s) were observed, suggesting decreased nonradiative E_{loss}s and implying a bigger room for improvement. It should be noted that BTP-4Cl has poor solubility due to the enhanced conjugated area caused by the replacement of fluorine by chlorine atoms. To improve the processability of BTP-4Cl, we then prolonged the alkyl chains of EH on the pyrrole rings (highlighted in red in Figure 1) to 2-bultyloctyl (BO) and 2-hexyldecyl (HD).[42] The modification of alkyl chains on pyrrole rings has a great impact on the solubility of this kind of molecules, which is consistent with the results reported by Zou et al.[31] As a result, the best photovoltaic performance was obtained by BTP-4Cl-BO with the BO chains. Here, in this contribution, we performed the third step modification by gradually decreasing the number of the carbon atoms on the edge of BTP-4Cl-BO (illustrated as green in Figure 1) to finely balance the relationship between processability and device efficiency. We replaced the C11 to C9 and then to C7, and as a result, we synthesized the BTP-eC9 and BTP-eC7. The synthetic procedures are quite similar for these NFAs, where the differences are only the selected alkyl bromides. The nuclear magnetic resonance and mass spectra characterizations are used to confirm the chemical structures of the NFAs. From simple solubility tests (Figure S2, Supporting Information), we find that these NFAs have a clear difference in solubility. BTP-eC11 and BTP-eC9 can be fully dissolved in common chlorobenzene (CB) and chloroform (CF) at a concentration of 15 mg mL^{-1} at 40 °C. Only BTP-eC11 can be fully dissolved in *o*-xylene (*o*-xy). However, the BTP-eC7 shows very limited solubility in common solutions at

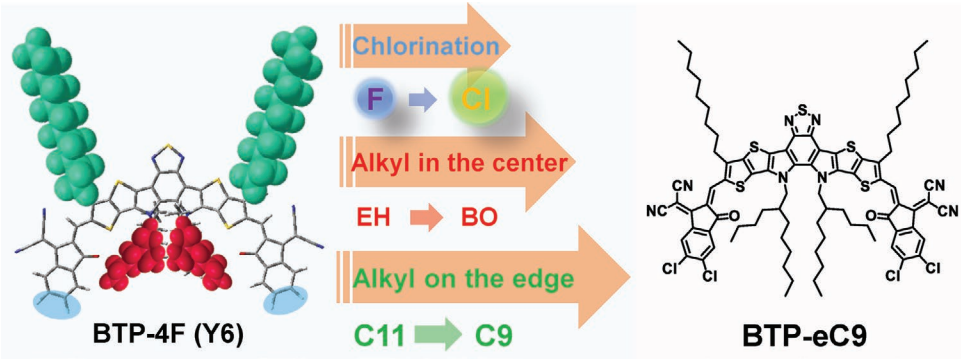

Figure 1. Illustration of the molecular configuration of Y6. Two kinds of alkyl chains (displayed in green and red) are highlighted by the space-filling model. The chemical modification on Y6 in our lab: fluorination to chlorination, optimization of the alky chains on the pyrrole, tune of the alkyl chains on the edge (this work, where C9 and C7 are used to replace the C11 to prepare the BTP-eC9 and BTP-eC7, respectively.)

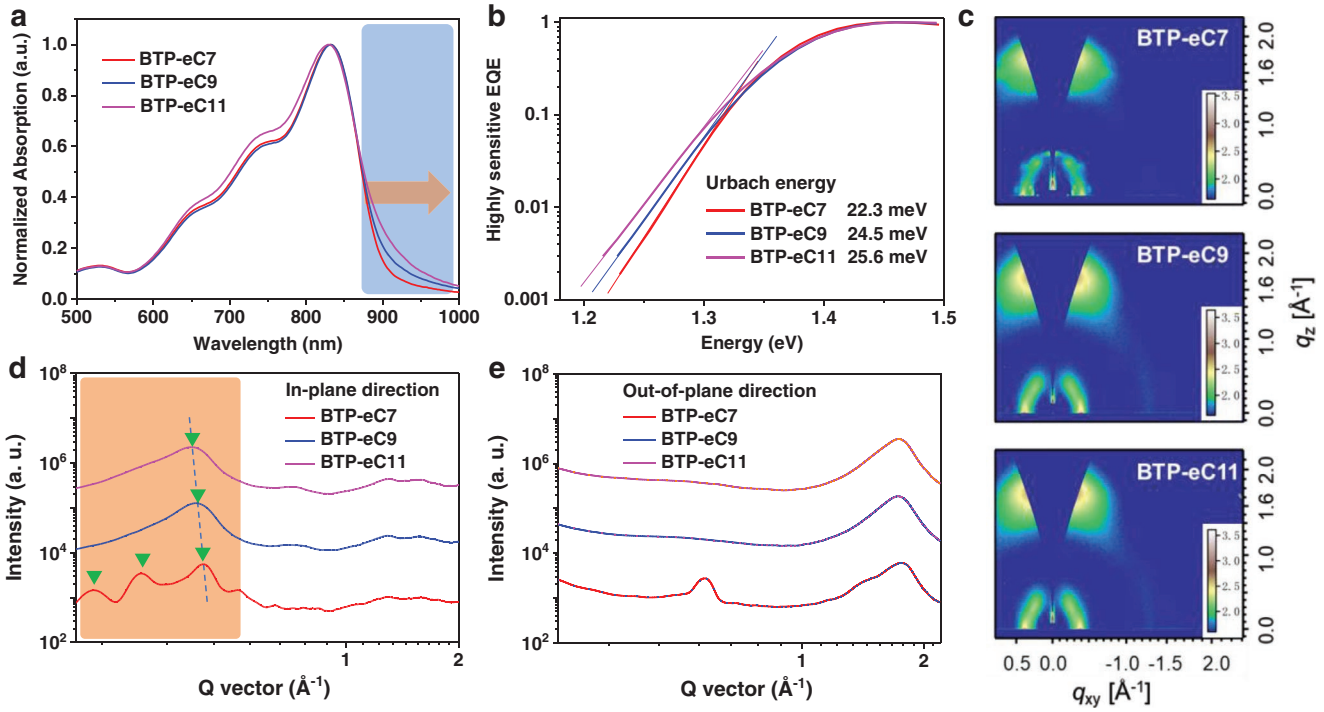

Figure 2. a) Normalized optical absorption spectra of the NFA films. b) Highly sensitive EQE spectra of the devices based on neat NFAs. c) 2D GIWAXS patterns of the NFA films. d) IP and e) OOP extracted line-cut profiles.

the same concentration, while high temperature (over 80 °C) CB is needed to dissolve it.

We first studied the impact of the alkyl chains on the absorption properties for the NFAs. In the diluted CF solutions, as displayed in Figure S3, Supporting Information, there is no obvious change for the three NFAs. From solutions to films (**Figure 2**a), the main absorption peaks of all the NFAs red-shift by ≈85 nm. It should be noted that, in the low photon energy range, the absorption tails are suppressed gradually for the NFAs with shortened alkyl chains. It implies that the localized states are decreased and should be associated with more ordered lamellar packing. We then measured the highly sensitive external quantum efficiency (EQE) spectra and calculated the Urbach energies (E_us) of the NFAs.[43] As plotted in Figure 2b, the calculated E_us are decreased gradually from 25.6 to 24.5, and to 22.3 meV for BTP-eC11, BTP-eC9, and BTP-eC7, respectively.

We further conducted the grazing-incidence wide-angle X-ray scattering (GIWAXS) measurements to investigate the intermolecular packing of the NFAs. The two-dimensional (2D) patterns shown in Figure 2c and the one-dimensional (1D) extracted profiles provided in Figures 2d,e display clear (010) peaks in the out-of-plane (OOP) direction, respectively, suggesting that all the NFAs prefer face-on orientations. From the in-plane (IP) profiles in the low-q region, we can find that the BTP-eC7 film shows multiple diffraction signals locating at 0.21, 0.28, and 0.42 Å^{-1}, demonstrating ordered structures with packing distances (d-spacing) of 29.9, 22.4, and 15.0 Å. For BTP-eC9 and BTP-eC11 films, However, there is only one diffraction peak left for BTP-eC9 and BTP-eC11 films, around 0.40 and 0.39 Å^{-1}, respectively, which suggests less ordered intermolecular stacking than BTP-eC7 film and is consistent with the results obtained from the absorption tails. The peaks at $q_{xy} \approx 0.42$ Å^{-1} in the neat NFA films are still maintained in the blend films with the polymer donor PBDB-TF (which will be discussed later), implying that these signals may be originated from the diffractions of backbone ordering. From the locations, the d-spacing of BTP-eC9 and BTP-eC11 films are estimated as 15.7 and 16.1 Å (Table S1, Supporting Information). According to the Scherrer equation, the coherence lengths (L_cs) are calculated to be 8.08, 5.19, and 4.41 nm. From the above results, we can rationally deduce that prolonging the alkyl chains on the edge of this kind of NFAs can "push away" the adjacent molecule to some extent. The subtle changes in d-spacing may affect the interaction of the electron-withdrawing terminal groups (which is believed to be the main interaction mode in this kind of NFAs), which may not only affect transport properties, but also blend morphology.[44]

In the OOP direction, BTP-eC7 film shows a smaller π–π d-spacing of 3.57 Å and a larger L_c of 1.99 nm than BTP-eC9 and BTP-eC11 films (d-spacing is 3.63 Å and L_c is 1.82 nm for both films). To estimate the charge transport property in the NFAs, we fabricated the electron-only devices using the structure of indium tin oxide (ITO)/ZnO/NFA/Al. By fitting the current density–voltage (J–V) curves in the space-charge-limited current region (Figure S4, Supporting Information), the electron mobilities of BTP-eC11, BTP-eC9, and BTP-eC7 are calculated to be 2.53×10^{-4}, 2.70×10^{-4}, and 1.28×10^{-4} cm^2 V^{-1} s^{-1}. The differences in electron mobility will be a crucial aspect that affects device performance.

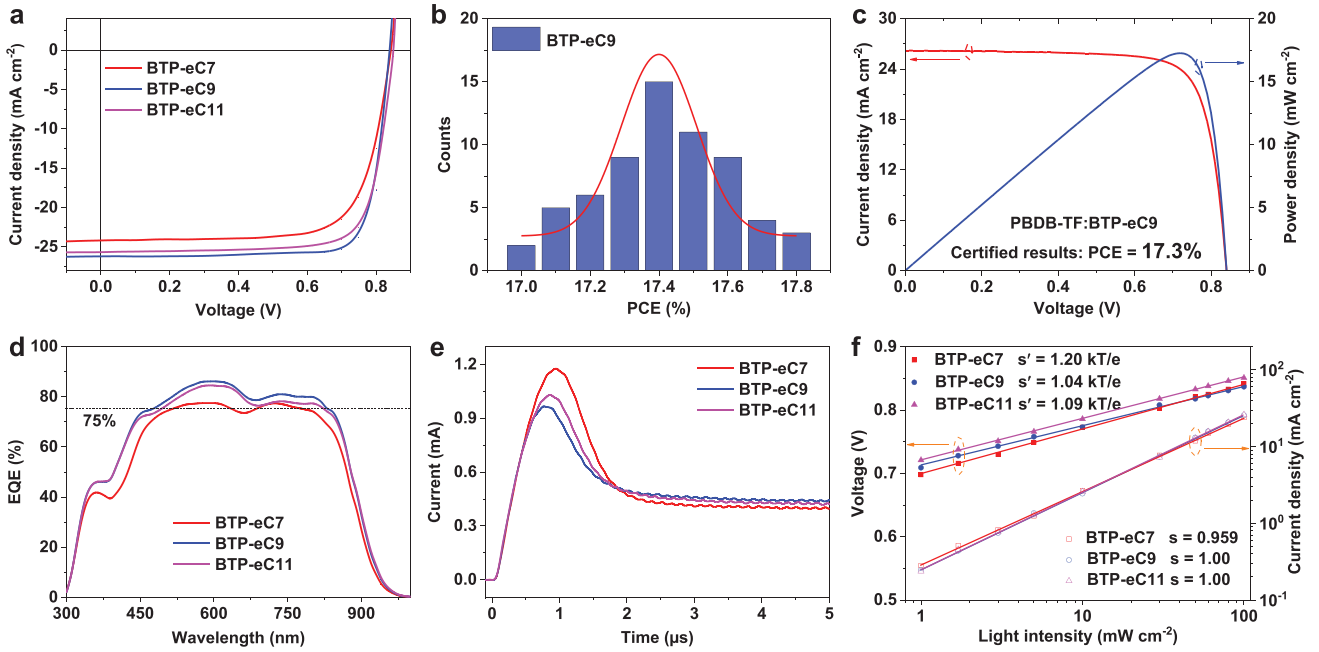

Figure 3. a) *J–V* curves of the optimal devices measured in our lab. b) Histogram of the PCEs of 64 devices. c) *J–V* and power density curves obtained in NIM. d) EQE curves of the optimal cells. e) Photo-CELIV curves of the devices. f) V_{OC} and J_{SC} dependence on P_{light}.

To investigate the photovoltaic properties of the NFAs, we fabricated the conventional OPV cells with a device configuration of ITO/PEDOT:PSS/donor:NFA/poly-[(9,9-bis(3′-((*N*,-*N*-dimethyl)-*N*-ethylammonium)-propyl)-2,7-fluorene)-*alt*-2,7-fluorene)-*alt*-2,7-(9,9-dioctylfluorene)]dibromide (PFN–Br)/Al, where a widely used polymer PBDB-TF was selected as donor. As the BTP-eC7-containing blend cannot be fully dissolved in CF, CB was used as the processing solvent, which is different from the other devices (where CF was used as the processing solvent). In addition to the host processing solvents, other device fabrication conditions are the same. The optimal *J–V* curves are plotted in **Figure 3**a and the detailed photovoltaic parameters are collected in **Table 1**. The device based on BTP-eC11 shows a PCE of 16.9% and the detailed parameters are close to the results in our previous report.[42] Impressively, a maximum PCE of 17.8% (V_{OC} = 0.839 V; J_{SC} = 26.2 mA cm^{-2}; FF = 0.811) is recorded for the BTP-eC9-based device. Figure 3b displays a histogram of PCEs for a population of 64 independent OPV cells from five batches. The PCEs are located in the range between 17.0% and 17.8% with a mean value of 17.4%. To confirm the photovoltaic performance by the independent certification laboratory, we first studied long-term stability of the device, and found that photovoltaic performance of the encapsulated devices only showed a slight decrease in a short time (Figure S5, Supporting Information). We sent our best cell to the National Institute of Metrology (NIM), China, and got a certified PCE of 17.3% (Figure 3c and Figure S6, Supporting Information). When compared to the BTP-eC11-based device, the improvements in J_{SC} and FF for the BTP-eC9-based device are the main reasons for its high PCE. The device containing BTP-eC7 yields a moderate PCE of 14.9% due to its relatively low J_{SC} of 24.1 mA cm^{-2} and FF of 0.735, which may be resulted from its poor blend morphology. By employing CF as a solvent, the device based on BTP-eC7

Table 1. Photovoltaic parameters of the OPV cells based on PBDB-TF:NFAs.

Process	NFA	V_{OC} [V]	J_{SC} [mA cm^{-2}][b)]	FF	PCE [%][c)]
Spin-coating method 0.09 cm^2	BTP-eC7	0.843	24.1 (23.6)	0.735	14.9 (14.4 ± 0.3)
	BTP-eC9	0.839	26.2 (25.9)	0.811	17.8 (17.4 ± 0.2)
	BTP-eC9[a)]	0.841	26.2	0.783	17.3
	BTP-eC11	0.851	25.7 (25.4)	0.775	16.9 (16.5 ± 0.2)
Blade-coating method 1 cm^2	BTP-eC7	0.809	20.3	0.533	8.75 (7.42 ± 0.7)
	BTP-eC9	0.832	25.7	0.759	16.2 (15.5 ± 0.4)
	BTP-eC11	0.843	25.3	0.722	15.4 (14.8 ± 0.4)

[a)]The certified result from NIM, China; [b)]Calculated current density by EQE curves shown in the brackets; [c)]The average PCEs are calculated from more than 20 independent cells.

achieves an awful PCE of 6.94% (Figure S7 and Table S2, Supporting Information).

According to the reported method, we measured the highly sensitive EQE and electroluminescence quantum efficiency (EQE_{EL}) of the OPV cells to analyze the E_{loss}s (Figure S8, Supporting Information). As collected in Table S3, Supporting Information, the three devices show very small differences in radiative and nonradiative recombination losses and overall E_{loss}s are approximately 0.55 eV. Figure 3d shows the EQE spectra of the optimal OPV cells. We can find that all the devices have over 75% EQE in the main absorption region of 450–850 nm. The overall EQE values of BTP-eC9- and BTP-eC11-based devices are much higher than those in BTP-eC7-based cells. The BTP-eC9-based device has the highest EQE value. The calculated integrated current densities are 23.6, 25.9, and 25.4 mA cm^{-2} for BTP-eC7-, BTP-eC9-, and BTP-eC11-based devices, respectively, which have good consistency with the *J*–*V* measurements.

To explore the reason for the improvement in BTP-eC9-based OPV cells, we evaluated the carrier transport and recombination properties in these devices. First, we conducted the photoinduced charge–carrier extraction in linearly increasing voltage (photo-CELIV) measurements to get the mobility of the faster carrier component in the working OPV cells. Calculated from the curves shown in Figure 3e, the charge mobilities are 1.13×10^{-4}, 2.78×10^{-4}, and 2.54×10^{-4} cm^2 V^{-1} s^{-1} for the devices based on BTP-eC7, BTP-eC9, and BTP-eC11.

We then measured the OPV cells via varying the light intensity (P_{light}) from 1 to 100 mW cm^{-2} and analyzed the impact of the P_{light} on the photovoltaic parameters (J_{SC} and V_{OC}) (Figure 3f). The P_{light} dependence of J_{SC} is described as $J_{SC} \propto P_{light}^{s}$, where the power-law exponent *s* reflects the bimolecular charge recombination condition in the device. All the devices show *s* values equal or close to unit, suggesting weak bimolecular recombination. By contrast, the BTP-eC9- and BTP-eC11-based OPV cells are better than the BTP-eC7-based device. The slope (*s*') of ΔV_{OC} versus $\Delta \ln(P_{light})$ is recognized as a good indication of the trap-state assisted charge recombination. The calculated *s*' values are 1.20, 1.04, and 1.09 kT e^{-1} for BTP-eC7, BTP-eC9, and BTP-eC11-based devices, respectively. The smallest *s*' value in BTP-eC9-based device implies that the most suppressed trap assisted charge recombination, partially contributing to its improved photovoltaic efficiency. The more serious charge recombination in the BTP-eC7-based device should be connected to its decreased performance and result from the unsuitable morphology.

We performed the morphology characterization on the active layer films using atomic force microscopy (AFM) and GIWAXS. As displayed in **Figure 4**, we can find the BTP-eC9 and BTP-eC11-based blend films possess a smooth surface with mean-square surface roughness (R_q) of approximately 1 nm. In the phase images, both the films show fiber-like domains with appropriate size. The nanoscale phase-separated morphologies are quite similar to our previous reports and should be closely dependent on the aggregation feature of the polymer donor PBDB-TF. Differently, the BTP-eC7-containing blend film shows a rough surface with a large R_q of 4.57 nm and excessive aggregation domains, which should result from the strong crystalline property and the low solubility of BTP-eC7. The strong crystalline property is associated with a large coherence length,

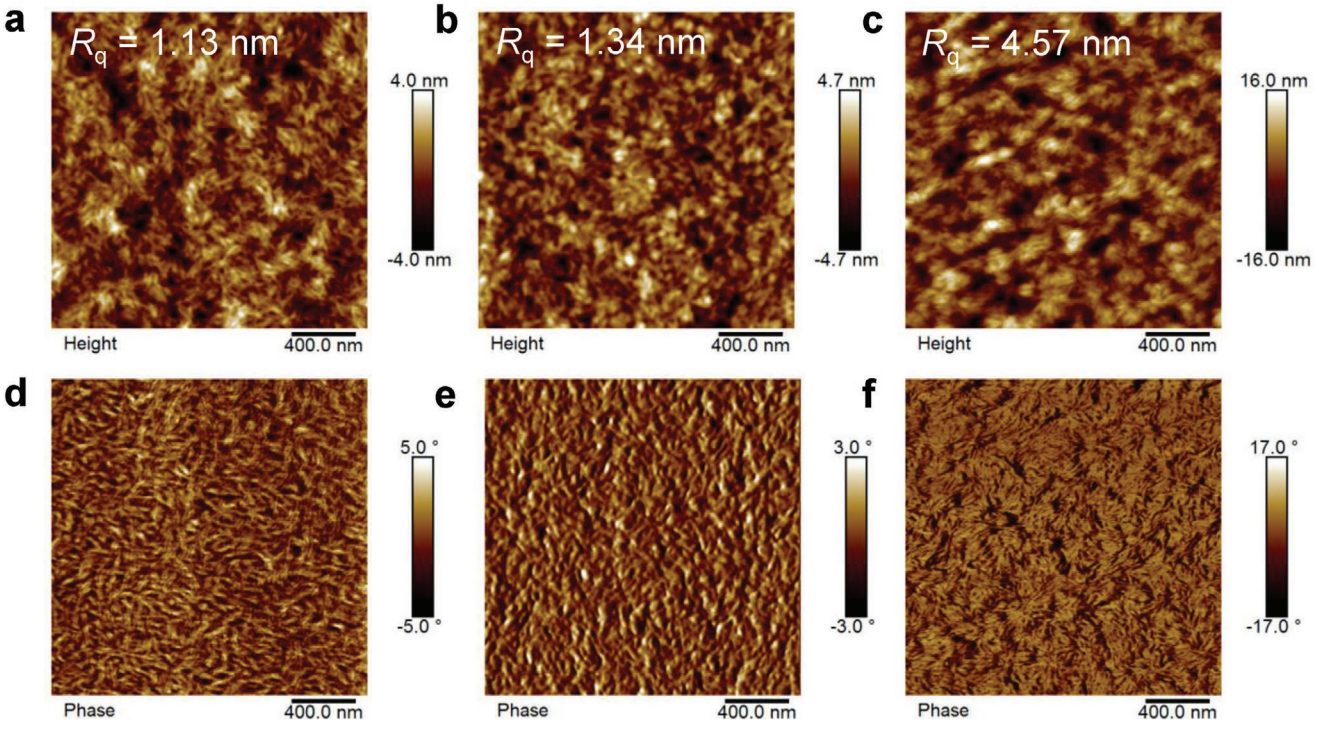

Figure 4. a–c) AFM height images of: a) PBDB-TF:BTP-eC11, b) PBDB-TF:BTP-eC9, and c) PBDB-TF:BTP-eC7 blend films. d–f) AFM phase images of: d) PBDB-TF:BTP-eC11, e) PBDB-TF:BTP-eC9, and f) PBDB-TF:BTP-eC7 blend films.

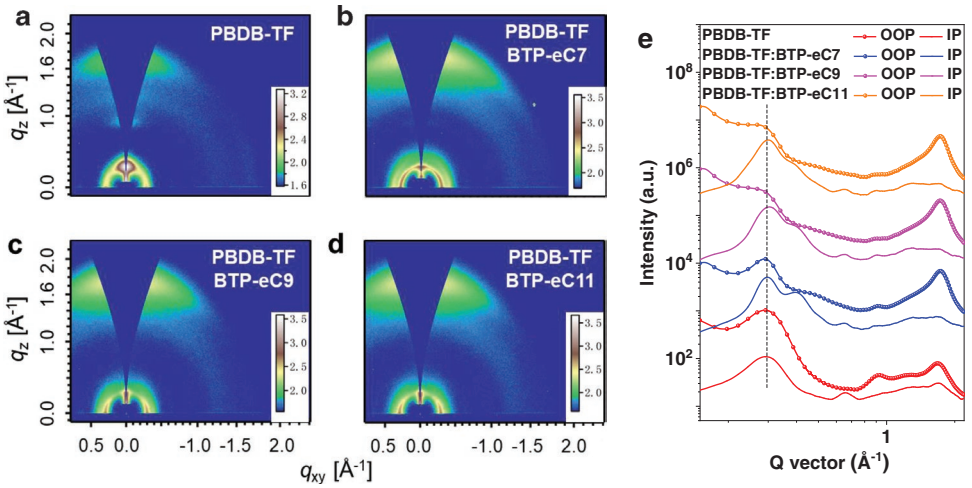

Figure 5. a–e) 2D GIWAXS patterns of: 2D GIWAXS patterns of: a) PBDB-TF, b) PBDB-TF:BTP-eC7, c) PBDB-TF:BTP-eC9, and d) PBDB-TF:BTP-eC11. e) 1D cut-line profiles of the PBDB-TF and PBDB-TF:NFAs.

which leads to large domain size. Therefore, an uneven surface may be formed between different phases.[15] This explains the severe charge recombination and thus moderate photovoltaic efficiency in the corresponding OPV cell.

The 2D GIWAXS patterns of the neat PBDB-TF and blend films are shown in **Figure 5**a and b–d, respectively. The extracted 1D profiles are displayed in Figure 5e. We can find that polymer donor PBDB-TF also adopts the face-on orientation. The OOP and the IP peaks locate at 1.68 and 0.29 Å^{-1}, respectively. Blending PBDB-TF with the NFAs does not change their face-on orientations. Interestingly, in the IP direction with low-q values, there are two distinct signals. In detail, the one with high intensity ($q_{xy} \approx 0.3$ Å^{-1}) should come from PBDB-TF, while the one with low intensity ($q_{xy} \approx 0.4$ Å^{-1}) should be derived from the NFA. The calculated L_c of PBDB-TF:BTP-eC7 blend film is 4.6 nm, which is much higher than that in PBDB-TF:BTP-eC9 (3.2 nm) and PBDB-TF:BTP-eC11 (3.0 nm) blend films, agreeing very well with the observations in the AFM measurements. In the OOP direction, the (010) peaks belonging to PBDB-TF and NFAs are highly overlapped. The calculated (010) L_cs are approximately 2 nm. The crystalline property implies a different degree of molecular ordered packing, which is correlated to the Urbach energy.[45,46] Here, the crystalline property of the three blend films is affected by the polymer donor PBDB-TF as it has a strong self-aggregation effect.[47,48] As a result, the Urbach energy of all blend films is similar (Figure S8, Supporting Information).

Since the large-area process is very important for the future industrial application, we also fabricated the 1 cm^2 devices by the blade-coating method. The fabrication procedures of the devices are provided in the Supporting Information. As shown in Table 1 and Figure S9, Supporting Information, the blade-coated device based on BTP-eC9 demonstrates an excellent PCE of 16.2%. For the device based on BTP-eC11, a PCE of 15.4% was obtained, which is similar to our previous result.[42] Both BTP-eC9 and BTP-eC11 show outstanding scale-up performance of OPV cells. However, due to the decreased volatilization rate of the solvent, the relatively low solubility of BTP-eC7 makes it easily dissolve out from the mixed solution. The BTP-eC7-based film has a large number of particles that can be seen by the human eye. In addition, strong crystalline property results in excessive aggregation (Figure S10, Supporting Information). As a result, the BTP-eC7-based device only achieves a PCE of 8.75%.

To conclude, we finely optimized the alkyl chain on the edge of the Y6-type molecule and studied the applications of the resulting NFAs in fabricating highly efficient OPV cells. By gradually shortening the alkyl chains of C11 to C9, then C7, we synthesized the NFAs of BTP-eC9 and BTP-eC7. The BTP-eC9 maintains good solubility and meanwhile possesses enhanced intermolecular ordering. The better morphology features improve the charge transport and suppress the charge recombination in the BTP-eC9-based device. As a result, the optimal OPV cells obtain an outstanding PCE of 17.8% (17.4 ± 0.2%, certified as 17.3%), which is among the top results in OPV cells. For BTP-eC7, it has low solubility and excessive aggregation in the blend, hurting the photovoltaic efficiency in the device. These results demonstrate that subtly optimizing the chemical structures of the OPV materials with excellent conjugated backbones is of great significance to fully explore their photovoltaic performance. We believe the further improvement in PCE can be achieved by rationally device engineering such as adopting multiple blending of donors or acceptors, controlling the blend morphology, and selecting efficient interlayers.

Supporting Information

Supporting Information is available from the Wiley Online Library or from the author.

Acknowledgements

This work was supported by the National Key Research and Development Program of China (No. 2019YFA0705900) funded by MOST and the Basic and Applied Basic Research Major Program of Guangdong Province (No. 2019B030302007). H.Y. acknowledges the financial support from the NSFC (21805287) and the Youth Innovation Promotion Association CAS (No. 2018043). J.H. would like to acknowledge the financial support from National Natural Science Foundation of China

(NSFC, 21835006, 91633301, 51961135103, and 51673201). C.H. was supported by NSFC (21734008). Y.C. thanks China Postdoctoral Science Foundation (2019M660800). F.G. acknowledges the financial support from the Swedish Research Council VR (2018-06048) and the Swedish Energy Agency Energimyndigheten (2016-010174). This work was also supported by the Beijing National Laboratory for Molecular Sciences (BNLMS-CXXM-201903).

Conflict of Interest

The authors declare no conflict of interest.

Keywords

molecular modification, nonfullerene acceptors, organic photovoltaic cells, power conversion efficiency

Received: December 13, 2019
Revised: February 13, 2020
Published online:

[1] S. Dai, X. Zhan, *Adv. Energy Mater.* **2018**, *8*, 1800002.
[2] R. Søndergaard, M. Hösel, D. Angmo, T. T. Larsen-Olsen, F. C. Krebs, *Mater. Today* **2012**, *15*, 36.
[3] H. Kang, G. Kim, J. Kim, S. Kwon, H. Kim, K. Lee, *Adv. Mater.* **2016**, *28*, 7821.
[4] M. Kaltenbrunner, M. S. White, E. D. Glowacki, T. Sekitani, T. Someya, N. S. Sariciftci, S. Bauer, *Nat. Commun.* **2012**, *3*, 770.
[5] F. C. Krebs, *Sol. Energy Mater. Sol. Cells* **2009**, *93*, 394.
[6] X. Meng, L. Zhang, Y. Xie, X. Hu, Z. Xing, Z. Huang, C. Liu, L. Tan, W. Zhou, Y. Sun, W. Ma, Y. Chen, *Adv. Mater.* **2019**, *31*, 1903649.
[7] C. Sun, R. Xia, H. Shi, H. Yao, X. Liu, J. Hou, F. Huang, H.-L. Yip, Y. Cao, *Joule* **2018**, *2*, 1816.
[8] J. Zhang, H. S. Tan, X. Guo, A. Facchetti, H. Yan, *Nat. Energy* **2018**, *3*, 720.
[9] C. Yan, S. Barlow, Z. Wang, H. Yan, A. K. Y. Jen, S. R. Marder, X. Zhan, *Nat. Rev. Mater.* **2018**, *3*, 18003.
[10] C.-Y. Liao, Y. Chen, C.-C. Lee, G. Wang, N.-W. Teng, C.-H. Lee, W.-L. Li, Y.-K. Chen, C.-H. Li, H.-L. Ho, P. H.-S. Tan, B. Wang, Y.-C. Huang, R. M. Young, M. R. Wasielewski, T. J. Marks, Y.-M. Chang, A. Facchetti, *Joule* **2020**, *4*, 189.
[11] T. W. Chen, C. C. Chang, Y. T. Hsiao, C. Chan, L. Hong, L. Zhong, W. T. Chuang, J. Hou, Y. Li, C. S. Hsu, *ACS Appl. Mater. Interfaces* **2019**, *11*, 31069.
[12] M. C. Scharber, D. Mühlbacher, M. Koppe, P. Denk, C. Waldauf, A. J. Heeger, C. J. Brabec, *Adv. Mater.* **2006**, *18*, 789.
[13] G. Li, Y. Yao, H. Yang, V. Shrotriya, G. Yang, Y. Yang, *Adv. Funct. Mater.* **2007**, *17*, 1636.
[14] D. Chen, F. Liu, C. Wang, A. Nakahara, T. P. Russell, *Nano Lett.* **2011**, *11*, 2071.
[15] G. Li, V. Shrotriya, J. Huang, Y. Yao, T. Moriarty, K. Emery, Y. Yang, *Nat. Mater.* **2005**, *4*, 864.
[16] W. L. Ma, C. Y. Yang, X. Gong, K. Lee, A. J. Heeger, *Adv. Funct. Mater.* **2005**, *15*, 1617.
[17] Y. Li, *Acc. Chem. Res.* **2012**, *45*, 723.
[18] L. Dou, Y. Liu, Z. Hong, G. Li, Y. Yang, *Chem. Rev.* **2015**, *115*, 12633.
[19] L. Lu, T. Zheng, Q. Wu, A. M. Schneider, D. Zhao, L. Yu, *Chem. Rev.* **2015**, *115*, 12666.
[20] D. Deng, Y. Zhang, J. Zhang, Z. Wang, L. Zhu, J. Fang, B. Xia, Z. Wang, K. Lu, W. Ma, Z. Wei, *Nat. Commun.* **2016**, *7*, 13740.
[21] Y. Liu, J. Zhao, Z. Li, C. Mu, W. Ma, H. Hu, K. Jiang, H. Lin, H. Ade, H. Yan, *Nat. Commun.* **2014**, *5*, 5293.
[22] J. Liu, S. Chen, D. Qian, B. Gautam, G. Yang, J. Zhao, J. Bergqvist, F. Zhang, W. Ma, H. Ade, O. Inganäs, K. Gundogdu, F. Gao, H. Yan, *Nat. Energy* **2016**, *1*, 16089.
[23] Y. Lin, J. Wang, Z. G. Zhang, H. Bai, Y. Li, D. Zhu, X. Zhan, *Adv. Mater.* **2015**, *27*, 1170.
[24] Y. Cui, H. Yao, L. Hong, T. Zhang, Y. Xu, K. Xian, B. Gao, J. Qin, J. Zhang, Z. Wei, J. Hou, *Adv. Mater.* **2019**, *31*, 1808356.
[25] J. Yuan, Y. Zhang, L. Zhou, G. Zhang, H.-L. Yip, T.-K. Lau, X. Lu, C. Zhu, H. Peng, P. A. Johnson, M. Leclerc, Y. Cao, J. Ulanski, Y. Li, Y. Zou, *Joule* **2019**, *3*, 1140.
[26] J. Yuan, T. Huang, P. Cheng, Y. Zou, H. Zhang, J. L. Yang, S.-Y. Chang, Z. Zhang, W. Huang, R. Wang, D. Meng, F. Gao, Y. Yang, *Nat. Commun.* **2019**, *10*, 570.
[27] J. Yuan, Y. Zhang, L. Zhou, C. Zhang, T. K. Lau, G. Zhang, X. Lu, H. L. Yip, S. K. So, S. Beaupre, M. Mainville, P. A. Johnson, M. Leclerc, H. Chen, H. Peng, Y. Li, Y. Zou, *Adv. Mater.* **2019**, *31*, 1807577.
[28] B. Fan, D. Zhang, M. Li, W. Zhong, Z. Zeng, L. Ying, F. Huang, Y. Cao, *Sci. China: Chem.* **2019**, *62*, 746.
[29] A. Karki, J. Vollbrecht, A. L. Dixon, N. Schopp, M. Schrock, G. N. M. Reddy, T. Q. Nguyen, *Adv. Mater.* **2019**, *31*, 1903868.
[30] Y. Cui, H. Yao, J. Zhang, T. Zhang, Y. Wang, L. Hong, K. Xian, B. Xu, S. Zhang, J. Peng, Z. Wei, F. Gao, J. Hou, *Nat. Commun.* **2019**, *10*, 2515.
[31] K. Jiang, Q. Wei, J. Y. L. Lai, Z. Peng, H. K. Kim, J. Yuan, L. Ye, H. Ade, Y. Zou, H. Yan, *Joule* **2019**, *3*, 3020.
[32] J. Song, C. Li, L. Zhu, J. Guo, J. Xu, X. Zhang, K. Weng, K. Zhang, J. Min, X. Hao, Y. Zhang, F. Liu, Y. Sun, *Adv. Mater.* **2019**, *31*, 1905645.
[33] C. Sun, F. Pan, S. Chen, R. Wang, R. Sun, Z. Shang, B. Qiu, J. Min, M. Lv, L. Meng, C. Zhang, M. Xiao, C. Yang, Y. Li, *Adv. Mater.* **2019**, *31*, 1905480.
[34] X. Xu, K. Feng, Z. Bi, W. Ma, G. Zhang, Q. Peng, *Adv. Mater.* **2019**, *31*, 1901872.
[35] J. Xiong, K. Jin, Y. Jiang, J. Qin, T. Wang, J. Liu, Q. Liu, H. Peng, X. Li, A. Sun, X. Meng, L. Zhang, L. Liu, W. Li, Z. Fang, X. Jia, Z. Xiao, Y. Feng, X. Zhang, K. Sun, S. Yang, S. Shi, L. Ding, *Sci. Bull.* **2019**, *64*, 1573.
[36] A. T. Yiu, P. M. Beaujuge, O. P. Lee, C. H. Woo, M. F. Toney, J. M. Frechet, *J. Am. Chem. Soc.* **2012**, *134*, 2180.
[37] B. Jang, C. Lee, Y. W. Lee, D. Kim, M. A. Uddin, F. S. Kim, B. J. Kim, H. Y. Woo, *Chin. J. Chem.* **2018**, *36*, 199.
[38] Y. Yang, Z. G. Zhang, H. Bin, S. Chen, L. Gao, L. Xue, C. Yang, Y. Li, *J. Am. Chem. Soc.* **2016**, *138*, 15011.
[39] J. Zhou, Y. Zuo, X. Wan, G. Long, Q. Zhang, W. Ni, Y. Liu, Z. Li, G. He, C. Li, B. Kan, M. Li, Y. Chen, *J. Am. Chem. Soc.* **2013**, *135*, 8484.
[40] T. Lei, J. H. Dou, J. Pei, *Adv. Mater.* **2012**, *24*, 6457.
[41] J. Zhao, Y. Li, G. Yang, K. Jiang, H. Lin, H. Ade, W. Ma, H. Yan, *Nat. Energy* **2016**, *1*, 15027.
[42] Y. Cui, H. Yao, L. Hong, T. Zhang, Y. Tang, B. Lin, K. Xian, B. Gao, C. An, P. Bi, W. Ma, J. Hou, *Natl. Sci. Rev.* **2019**, https://doi.org/10.1093/nsr/nwz200.
[43] V. C. Nikolis, A. Mischok, B. Siegmund, J. Kublitski, X. Jia, J. Benduhn, U. Hormann, D. Neher, M. C. Gather, D. Spoltore, K. Vandewal, *Nat. Commun.* **2019**, *10*, 3706.
[44] H. Bristow, K. J. Thorley, A. J. P. White, A. Wadsworth, M. Babics, Z. Hamid, W. Zhang, A. F. Paterson, J. Kosco, J. Panidi, T. D. Anthopoulos, I. McCulloch, *Adv. Electron. Mater.* **2019**, *5*, 1900344.
[45] H. Mehdizadeh-Rad, J. Singh, *ChemPhysChem* **2019**, *20*, 2712.
[46] A. Yin, D. Zhang, S. H. Cheung, S. K. So, Z. Fu, L. Ying, F. Huang, H. Zhou, Y. Zhang, *J. Mater. Chem. C* **2018**, *6*, 7855.
[47] J. Hou, O. Inganas, R. H. Friend, F. Gao, *Nat. Mater.* **2018**, *17*, 119.
[48] H. Zhang, H. Yao, J. Hou, J. Zhu, J. Zhang, W. Li, R. Yu, B. Gao, S. Zhang, J. Hou, *Adv. Mater.* **2018**, *30*, 1800613.

